

Additive-Free Morphology Controlled Synthesis of Hierarchical Lithium Iron Phosphate Mesosturctures

Nan Zhou^{1,2}, Hai-Yan Wang¹, Su-Qin Liu¹, Guozhong Cao², and You-Nian Liu^{1,*}

¹ College of Chemistry and Chemical Engineering, Central South University, Changsha, Hunan, 410083, China.

² Department of Materials Science and Engineering, University of Washington, Seattle, Washington, 98195, United States.

*E-mail: liyounian@csu.edu.cn

Received: 23 March 2013 / Accepted: 25 April 2013 / Published: 1 July 2013

Three dimensional hierarchical lithium iron phosphate mesostructures were successfully fabricated through a simple solvothermal synthesis by using the mixture of ethylene glycol/dimethylacetamide/water (EG/DMAC/H₂O) as co-solvent. No other surfactant or template agent was applied. For the authors' best knowledge, it is the first application of EG/DMAC/H₂O mixture as co-solvent for the synthesis of cathode materials as LiFePO₄ for lithium ion batteries. Hierarchical LiFePO₄ mesostructures with different morphology and size can be synthesized by adjusting the ratio of the EG/DMAC/H₂O co-solvent. Palma-like, dumbbell-like and urchin-like hierarchical LiFePO₄ mesostructures with different small-sized building blocks were finally obtained. The characteristics and electrochemical performance of the obtained three LiFePO₄ mesostructures were investigated. It is found that the size of the whole structure and building blocks has a great affection on the electrochemical performance of the LiFePO₄ mesostructures at low rate condition. Among the three LiFePO₄ mesostructures, the urchin-like mesostructure composed of LiFePO₄ nanoplates showed the best initial lithium intercalation property of 103 mAh g⁻¹ at a current density of 17 mA g⁻¹ (0.1 C) without any conductive coating, which should be attributed to the high specific surface area and high porosity introduced by the special superstructure and well crystallized LiFePO₄ nanoplates composition units.

Keywords: mesostructures; LiFePO₄; morphology control; lithium ion battery; cathode

1. INTRODUCTION

Owing to numerous appealing features such as high theoretical capacity (170 mA h g⁻¹), abundant raw material thus low cost, environment friendly and superior safety and stability[1], olivine lithium iron phosphate (LiFePO₄ or in short LFP hereafter) has been attracting extensive attentions as a

potential cathode material for new generation lithium ion batteries (LIBs). However, the main disadvantage of sluggish mass and low conductivity largely hindered the wide-spread application of LiFePO_4 [2-5]. Tremendous efforts such as conductive coating[6-8], cationic doping[9-11] and particle reducing[12-14] *etc.* have been made to address this problem. Decreasing the particle size to nanometer scale combined with controlling morphology of the whole structure is considered to be one of the most effective ways to improve the electrochemical performance of LFP materials[15]. Thus, hierarchically assembly LFP mesostructures with nanoscale building blocks, which introduces: a) large surface area to faster the intercalation/deintercalation reactions; b) high porosity to increase the interface between the electrode/electrolyte; c) small sized buck material with high crystallization to short the diffusion path of Li ions; and d) large mesostructure with micrometer scaled size to enhance the process ability; offers a new unique option for advanced LFP material design. Several hierarchical LiFePO_4 assemblies with different morphology have already been reported. For example, Qian *et al.*[16] fabricated nanoembossed LiFePO_4 microspheres with high porous structure, which allows easily carbon coating on the interior nano-plates of the microspheres thus excellent rate performance was obtained. Yang group[17] solvothermally synthesized dumbbell LiFePO_4 microstructures self-assembled by nano-plates with the application of poly(vinyl pyrrolidone) (PVP) as surfactant. Popovic *et al.*[18] synthesized urchin-like LFP mesostructures through a template-free solvothermal route, but low lithium intercalation capacity was obtained for this mesostructure even after carbon coating. Flower like LFP microstructures with good storage and cyclic performance were prepared through solvothermal route by Rangappa group[19]. However, expensive organic surfactants were applied for most of the aforementioned works, making the synthesis a very complicate process, and long reaction duration were needed. It is very important to explore a new effective way to synthesis hierarchical LiFePO_4 mesostructures with strong storage performance.

Numerous methods have been utilized to synthesize LiFePO_4 materials, such as solid-state reaction[20-23], chemical vapor deposition[24-26], carbothermal reducing[27, 28], co-precipitation[29-31], sol-gel synthesize[13, 32, 33], hydrothermal/solvothermal approach[19, 34-36], microwave processing[37-39], to name a few. Among them, solvothermal synthesis has been confirmed to be an efficient way to have phase purity, grain size and particle morphology controlled. Other than single aqueous solvent in hydrothermal processing, different environmental friendly solvents such as ethanol or ethylene glycol are utilized in solvothermal synthesis, by the absorption of solvent molecules onto particle surfaces during particle growth, allowing for the precise control over the particle size, product shape, and even crystallinity of metal oxide nanoparticles or nanostructures. Most hierarchical LFP mesostructures were synthesized via solvothermal route[17-19], as those aforementioned works. In addition, getting rid of water solvent can largely reduce the risk of iron hydroxide formation in precursor solution, which can greatly increase the phase purity of the final product[18].

Most recently, our group successfully fabricated hierarchical dumbbell-shaped LiFePO_4 mesocrystals via solvothermal synthesis by using dimethylformamide/ethylene glycol (DMF/EG) as co-solvent without any additive or surfactant[40]. The co-solvent DMF/EG played a crucial role in the formation of the dumbbell-shaped LFP mesostructures. The obtained hierarchical LiFePO_4 mesostructure and its in situ carbon coated counterpart show high lithium intercalation properties and

good cyclic stability. In this work, three-dimensional hierarchical LiFePO_4 mesostructures with controlled morphology were synthesized via solvothermal route by using ethylene glycol/dimethylacetamide/water (EG/DMAC/ H_2O) co-solvent without any surfactant or additive. To the authors' best knowledge, this is the first utilization of EG/DMAC/ H_2O mixture as co-solvent in the synthesis of cathode materials such as LiFePO_4 for lithium ion batteries. The morphology and composition units of LFP mesostructures can be controlled by adjusting the ratio of co-solvent. Three different shapes of palma-, dumbbell- and urchin-like products were finally obtained and the urchin-like LiFePO_4 mesostructures composed of nanoplates showed the best electrochemical performance.

2. EXPERIMENTAL

Synthesis: Lithium dihydrogen phosphate LiH_2PO_4 ($\geq 99.0\%$, Aesar) and Ferrers sulfate heptahydrate $\text{FeSO}_4 \cdot 7\text{H}_2\text{O}$ ($\geq 99.0\%$, Aldrich) were utilized as precursors to synthesis hierarchical LiFePO_4 mesostructures with different morphology. First, 0.8 m mol $\text{FeSO}_4 \cdot 7\text{H}_2\text{O}$ was dissolved in EG while stoichiometric amount of LiH_2PO_4 was dissolved in DMAC/ H_2O co-solvent separately. Then the two solutions were mixed together and ultrasonicated for 10 min to make a homogeneous mixture. The color of the reactants changed to grey blue as soon as they mixed together. The overall molar ratio of Li:Fe:P was 1 : 1 : 1. The ratio of the co-solvent for LFP mesostructures with different morphology are summarized in Table 1.

Table 1. Ratio of the co-solvent for LFP mesostructures with different morphology

Samples	Ratio of the co-solvent (ml)		
	H_2O	DMAC	EG
palma-like LFP mesostructures	0.6	3.4	6
dumbbell-like LFP mesostructures	0.6	4.2	5.2
urchin-like LFP mesostructures	1.1	4.45	4.45

The obtained mixture was transferred into a 30 ml PTFE inner steel autoclave and heated at 225 °C for 4 h. After that, the autoclave was taken out of the furnace and fast cooled to room temperature. The obtained product was washed with ethanol and de-ionized water several times. No other surfactants or template agents were added during the solvothermal process. All samples were annealed at 600 °C in inert gas environment for 5 h to guarantee better crystallinity.

Structural characterization and property measurements: Scanning electron microscopy (SEM, JEOL JSM-5200F) was performed to detect the morphology of the samples. X-Ray Diffraction (XRD, D8 Bruker) was carried out to determine the crystals phase of LFP mesostructures with different morphology. The obtained samples were mixed with super P carbon black and poly(vinyl difluoride) (PVDF) in the weight ratio of 75 : 15 : 10 with the solvent of N-methyl pyrrolidone (NMP). After that,

the mixture was pasted on an aluminum foil to fabricate composite electrodes. The electrode films were assembled into R2016 coin-type cells in an Argon filled glove box by using lithium metal foil, 1 M LiPF_6 in ethylene carbonate (EC)/dimethyl carbonate (DMC) (1 : 1, in weight) and Celgard 2400 membrane as counter electrode, electrolyte and separator respectively. Cyclic voltammetry (CV) were performed on a CHI660B electrochemical workstation (shanghai, China) at ambient temperature. Charging-discharging cycling tests of the assembled cells at a constant current mode were carried out using a computer controlled electrochemical analyzer (Land, China) in the voltage range of 4.2 - 2.5 V (vs. Li/Li^+)

3. RESULTS AND DISCUSSION

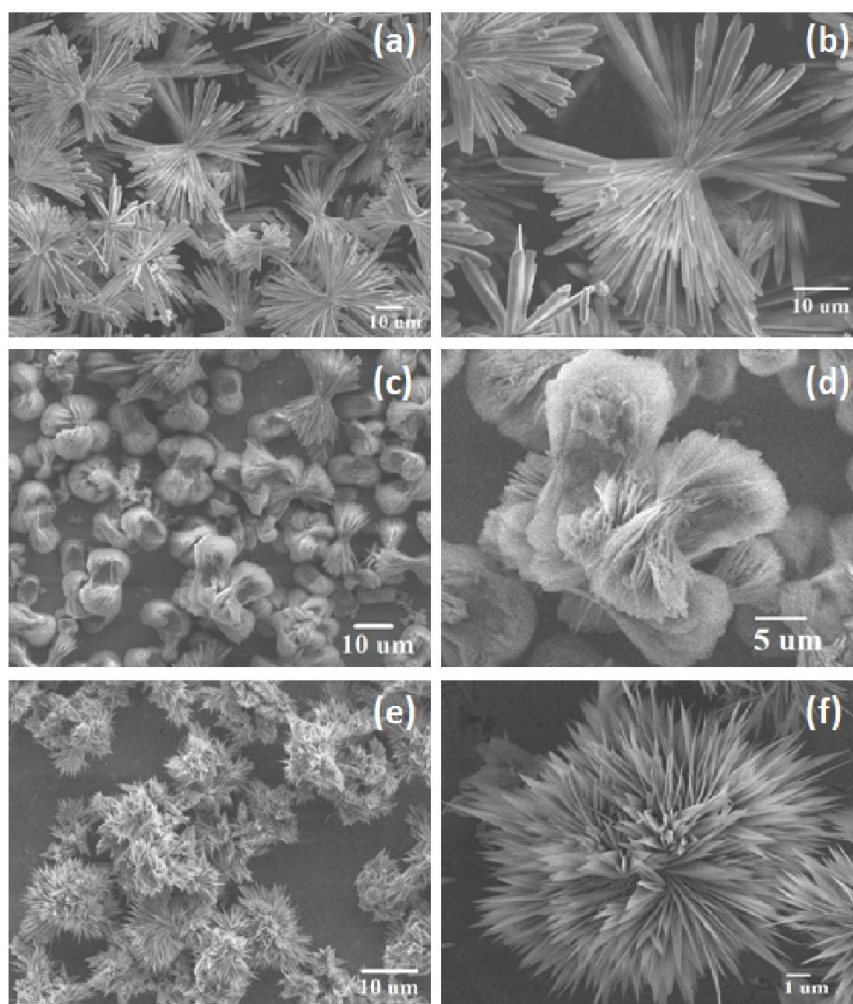


Figure 1. SEM images of hierarchical (a) (b) palma-like LiFePO_4 mesostructures (c) (d) dumbbell-like LiFePO_4 mesostructures (e) (f) urchin-like LiFePO_4 mesostructures

Figure 1 shows the SEM images of the obtained LiFePO_4 mesostructures at different magnifications. Three LiFePO_4 products with changed morphologies of palma-, dumbbell- and urchin-like shapes were successfully fabricated through solvothermal route by using the EG/DMAC/ H_2O co-

solvent for 4 hours, without any surfactant or additive. All of the obtained LiFePO_4 samples are uniformly-sized hierarchical three-dimensional mesostructures consist of small LiFePO_4 building blocks. As shown in Figure 1 (a) and (b), the palma-like LiFePO_4 mesostructures have a structure size around $25\ \mu\text{m}$ and looks like two palma leaves connected head to head. This mesostructures hold the largest size among the obtained three samples and are composed of micro-sized LFP rods with a length of $\sim 10\text{-}15\ \mu\text{m}$ and a diameter of about $1\text{-}1.5\ \mu\text{m}$. The obtained dumbbell-like LiFePO_4 mesostructures (Figure 1 (c) and (d)) have relatively smaller size around $18\ \mu\text{m}$. The primary units of this mesostructures are nano-sized LFP flat plates, which have a length of $15\text{-}20\ \mu\text{m}$ and a thickness of about $200\ \text{nm}$. Even smaller urchin-like LiFePO_4 mesostructures (Figure 1 (e) and (f)) were formed when the ratio of water went up to $1.1\ \text{ml}$ and equal $4.45\ \text{ml}$ amount of EG and DMAC was applied during the solvothermal process. This mesostructures with a $15\ \mu\text{m}$ size are composed by beautiful triangle shaped LiFePO_4 nano-plates with a thickness around $100\ \text{nm}$. With other parameters unchanged, hierarchical LiFePO_4 mesostructures with different shapes can be obtained by adjusting the ratio of the EG/DMAC/ H_2O co-solvent during the solvothermal synthesis. Thus, it can be concluded that the ratio of the co-solvent has great impact on the size and morphology of the LiFePO_4 mesostructures.

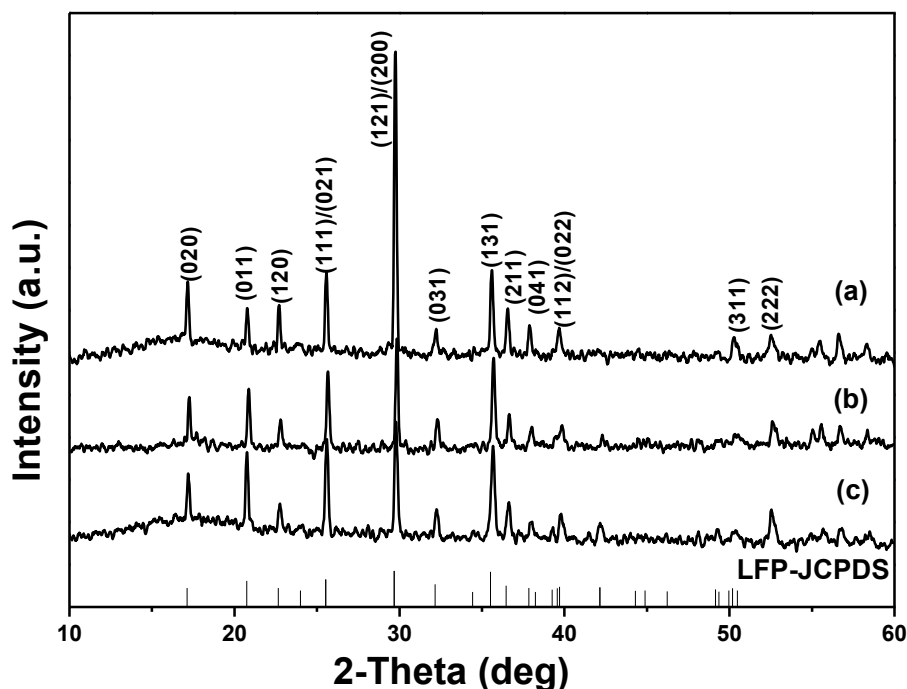


Figure 2. XRD patterns of hierarchical (a) palma-like LiFePO_4 mesostructures (b) dumbbell-like LiFePO_4 mesostructures (c) urchin-like LiFePO_4 mesostructures

XRD analysis were carried out to investigate the crystal phase of the obtained three hierarchical LiFePO_4 mesostructures with different morphology synthesized from solvothermal approach followed with further annealing at $600\ ^\circ\text{C}$ for $5\ \text{h}$, results shown in Figure 2. All XRD patterns for three samples are indexed to orthorhombic olivine based LiFePO_4 material (JCPDS card #040-1499) with good

crystallinity. No other secondary phases such as FeP, FePO₄ or Li₃PO₄ were detected. The lattice parameters of three LiFePO₄ mesostructures with various shapes are summarized in Table 2, all of them corroborate well with those values reported in literature[41]. Thus, it can be concluded that pure LiFePO₄ materials can be obtained during a simple solvothermal route by using EG/DMAC/H₂O co-solvent in a short reacting time of 4 h followed with calcinations at 600 °C for 5 h with no additive or surfactant.

Table 2. Lattice parameters for LFP mesostructures with different morphology

Samples	Lattice parameters		
	<i>a</i>	<i>b</i>	<i>c</i>
palma-like LiFePO ₄ mesostructures	10.3248 Å	5.9871 Å	4.6998 Å
dumbbell-like LiFePO ₄ mesostructures	10.2964 Å	5.9900 Å	4.7129 Å
urchin-like LiFePO ₄ mesostructures	10.3484 Å	5.9766 Å	4.7141 Å

It has been mentioned that the ratio of the EG/DMAC/H₂O co-solvent has great impact on the size and morphology of the LiFePO₄ mesostructures. However, the exactly mechanism of the formation of hierarchical LiFePO₄ mesostructures with different shapes remains unclear. Most of the aforementioned hierarchical LiFePO₄ mesoporous architectures are self-assembled from nano-sized composition unites combined with a phase transformation from Li₃PO₄ to LiFePO₄[17]. It should be noted that there are different opinions about the driving force of the self-assembly formation mechanism of hierarchical LFP mesostructures. Some attribute to the Van der Waals attraction as a result of hydrophobic interaction due to the bonded surfactant molecules at the end of the small units[42]. Another opinion is that the hierarchical mesostructure is the result of the aggregation of LFP small particles occurred during the synthesis process under Ostwald ripening and surface tension[43]. Others conclude that the hierarchical LFP mesostructures are re-crystallized from the 3D structured aggregates under lattice tension or surface interaction at the edge areas[17]. It is suggested that special surfactants played a crucial role in the formation of hierarchical mesoporous LFP architectures and were largely utilized in the hydro-/solvothermal synthesis of LFP mesostructures. However, hierarchical dumbbell-shaped LiFePO₄ mesocrystals can be successfully synthesized through solvothermal route by using DMF/EG co-solvents without any surfactant or additive[40]. The formation of the dumbbell-shaped mesostructures could possibly be a result of the cooperation of DMF/EG co-solvents, due to which interface energy, chemistry or ion diffusivity might have been applied during the formation process. In this work, hierarchical LFP mesostructures with different morphology were also obtained via solvothermal process with the application of the EG/DMAC/H₂O mixture, confirming the participation of co-solvent has great affection on the formation of LFP mesostructures. Unfortunately, the utilization of the mixture of three reagents of EG, DMAC and water during the synthesis makes the reaction between the reactants and solvents a very complicated process.

The mechanism of the formation of the hierarchical LiFePO_4 mesostructures with different morphology remains a challenge and still needs further investigation.

The three mesostructure samples were mixed with carbon black and binder to fabricate cathode films and assembled into R2016 coin-type cells in an Argon filled glove box respectively. Cyclic voltammetric (CV) analysis were performed to investigate the intrinsic kinetics of the three hierarchical LiFePO_4 mesostructures with different morphology. The CV analysis was taken out under a scanning rate of 0.1 mV S^{-1} within a voltage limit of 2.4 - 4.3 V and results shown in Figure 3. Only one pair of cathodic and anodic peaks appeared in the range of 3.2 - 3.6 V (vs. Li/Li^+) was detected for each sample, consistent with the two phase reaction of $\text{Fe}^{2+}/\text{Fe}^{3+}$, which is corresponding to the lithium ions intercalation and deintercalation of LiFePO_4 crystals respectively. All three CV curves show symmetry shape and area of the oxidation and reduction peaks respectively, suggesting the well reversibility of the hierarchical LiFePO_4 mesostructures. Among all the three samples, the hierarchical urchin-like LiFePO_4 mesostructures has the highest values of current peaks' magnitude when compared with the palma-like and dumbbell-like LFP mesostructures, indicating the urchin-like LFP mesostructures have better reaction kinetics than the other two samples. Similar values of current peaks' magnitude were found for the palma-like LFP mesostructure and the dumbbell-like LFP mesostructures. However, the palma-like LFP mesostructures exhibits an anodic peak at 3.64 V and a corresponding cathodic peak at 3.26 V, while the dumbbell-like LFP mesocrystals exhibits an anodic peak at 3.56 V and a corresponding cathodic peak at 3.31 V. The potential interval of the two mesostructures is 0.38 V and 0.25 V respectively. It is believed that more effective redox reactions would be detected when smaller potential interval between redox peaks of the material was found[44].

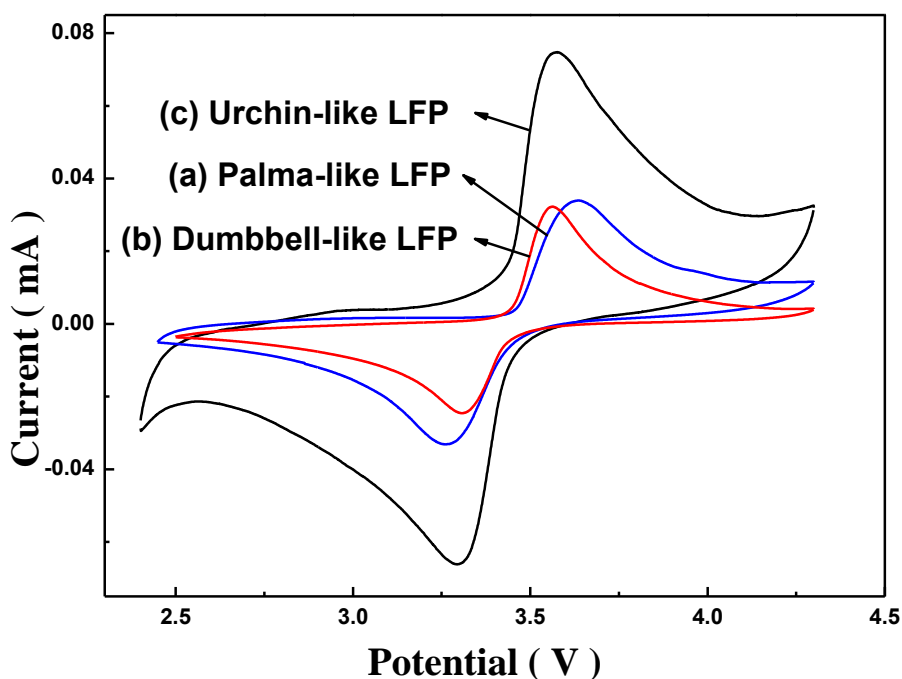
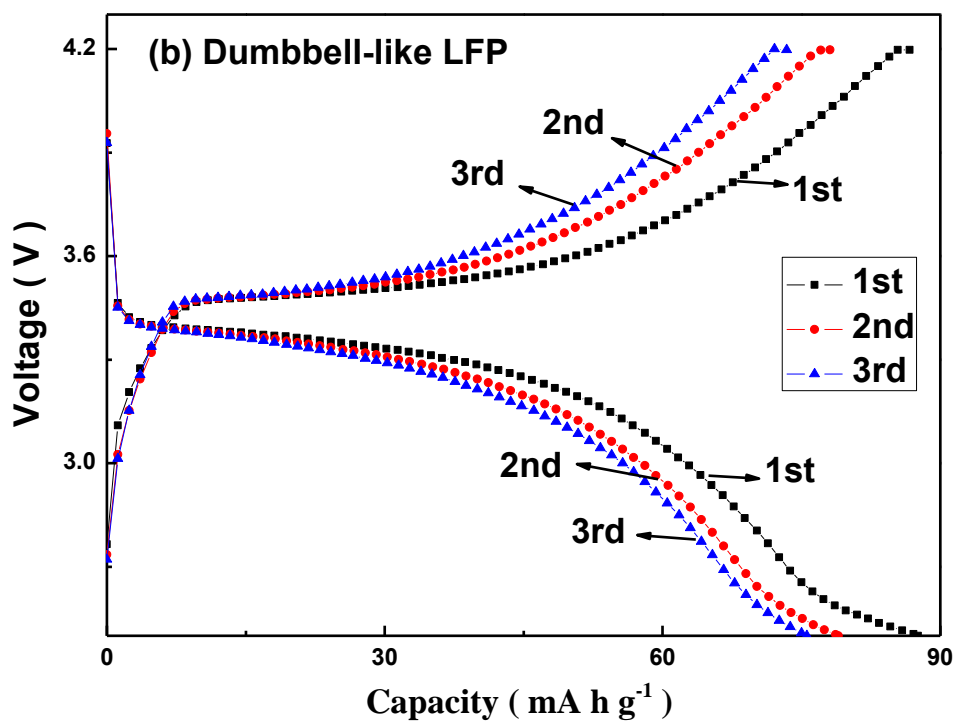
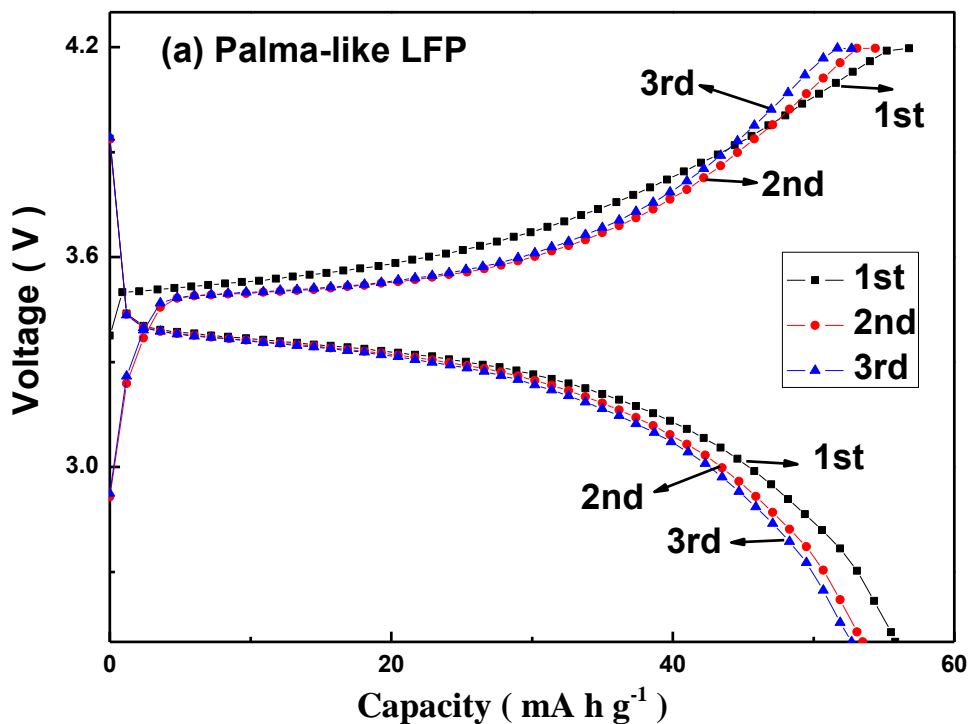


Figure 3. CV curves of hierarchical palma-like, dumbbell-like and urchin-like LiFePO_4 mesostructures under 0.1 mV S^{-1} scanning rate between 2.4 - 4.3V (vs. Li/Li^+)

It is likely that the hierarchical dumbbell-like LiFePO_4 mesostructures has faster reactions than the hierarchical palma-like LiFePO_4 mesostructures. This conclusion corroborates well with the profiles of lithium intercalation/deintercalation analysis discussed in next paragraph.



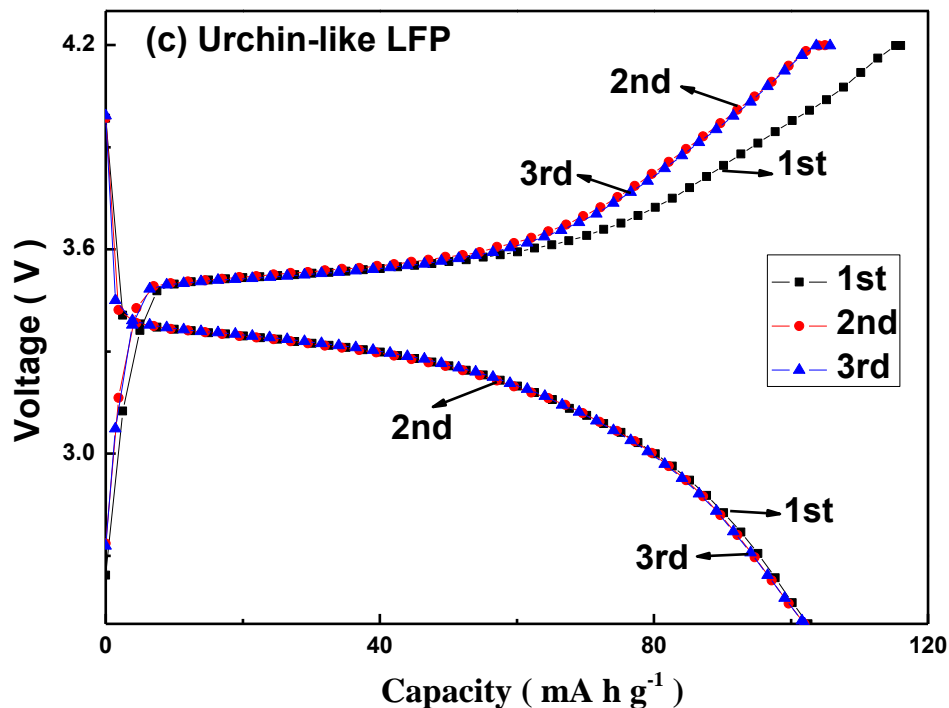


Figure 4. Initial three cycles of lithium ion charge-discharge process of (a) palma-like, (b) dumbbell-like and (c) urchin-like LFP mesostructures at 0.1C rate between 2.5 - 4.2V (vs. Li/Li^+)

Figure 4 shows the first three charge/discharge patterns of these hierarchical LiFePO_4 mesostructures with different morphology at a current density of 17 mA g^{-1} (0.1 C) in the voltage range of 2.5 V to 4.2 V (vs. Li/Li^+). The hierarchical palma-like LiFePO_4 mesostructures exhibited a poor charge capacity of about 56.8 mA h g^{-1} and discharge capacity of about 55.8 mA h g^{-1} (Figure 4 (a)) at the first cycle. For the next two cycles, although the gap between the charge and discharge curves narrowed and became steady, lower capacities around 53 mA h g^{-1} were found for both charge and discharge processes of this palma-like mesostructures. This poor lithium intercalation/deintercalation property is far beyond practical application. But even lower capacity was found in hierarchical urchin-like LiFePO_4 mesocrystals consisted of nano-sheets reported by Popovic group[18]. The author attributed the poor storage performance to the intrinsic low conductivity of the LFP material. However, higher initial charge and discharge capacity of 86.7 mA h g^{-1} and 87.6 mA h g^{-1} were exhibited by dumbbell-like LFP mesostructures (Figure 4 (b)) and even higher 116 mA h g^{-1} and $102.5 \text{ mA h g}^{-1}$ initial capacity were obtained for urchin-like LFP mesostructures (Figure 4 (c)). Besides, high lithium intercalation properties were reported for many pure hierarchical LiFePO_4 mesoporous architectures. For example, the pure mesoporous LiFePO_4 microspheres synthesized by Qian *et al.* [16] exhibited a 100 mA h g^{-1} at 0.1 C rate. An initial 110 mA h g^{-1} discharge capacity at 0.1 C rate was obtained for hierarchical dumbbell-shaped LiFePO_4 mesocrystals fabricated with DMF/EG co-solvent in our group[40]. It's worth noting that the urchin-like LFP mesocrystals with low 25 mA h g^{-1} discharge capacity reported by Popovic group[18] hold a structure size of about $40 \mu\text{m}$, while the mesoporous microspheres fabricated by Qian group[16] have an average diameter around $3 \mu\text{m}$. The dumbbell-shaped LFP mesocrystal have a smaller structure size $\sim 2\text{-}3 \mu\text{m}$ with a diameter of about $1.5 \mu\text{m}$ in the head and a diameter of about 300 nm in the middle. In this work, the palma-like

mesostructures have the largest size of about 25 μm among the three obtained samples and the primary unit of this architecture is micro-sized LFP rods with a diameter of about 1-1.5 μm . The dumbbell-like LFP mesostructures have a smaller size of about 18 μm with nano-sized LFP plate building blocks. The urchin-like LFP mesostructures have the smallest size of around 15 μm and the composition units of this sample are LFP nano-plates with a thickness about 100 nm. As we all know, enhance the diffusion of the Li^+ ions can greatly improve the electrochemical performance of LiFePO_4 material. It seems that the size of the whole structure and the primary units have great effect on the electrochemical property of the hierarchical mesoporous materials, since larger size will lead to super long diffusion path of lithium ions and retard the transfer of electrons. The charge/discharge property increased with the size decrease of the structures and the primary units, since lithium ions can be more easily intercalate/deintercalate from the interior part of the materials with smaller sizes.

Another thing needs to mention is that the charge and discharge curves of all three samples show longer slop regions and shorter flat plateaus when compared with conventional LiFePO_4 materials. Similar phenomenon has also been reported for other mesoporous architectures with high surface area and nano-sized particles[45, 46]. There are two possible explanations[19, 47]. Some think the longer slope appears due to the formation of a single-phase solid solution, which was found in nanostructures with particle size under 45 nm[48, 49]. In our work, all three samples have much larger particles than this critical size; it is unlikely to form the single-phase solid solution. The others attribute the slope to the capacitive behavior happens in the surface or interfacial of the material, which is named the pseudo-capacitive effect[50]. This effect happened to many materials with high surface area and nanostructures, and both surface capacitive adsorption and lithium ion intercalation contribute to the total storage capacitance[45, 46, 51, 52]. Since our products are all mesoporous structures with high surface area and nano-sized building blocks, the pseudo-capacitive effect is likely to happen and leading to the longer slope region of all charge/discharge curves.

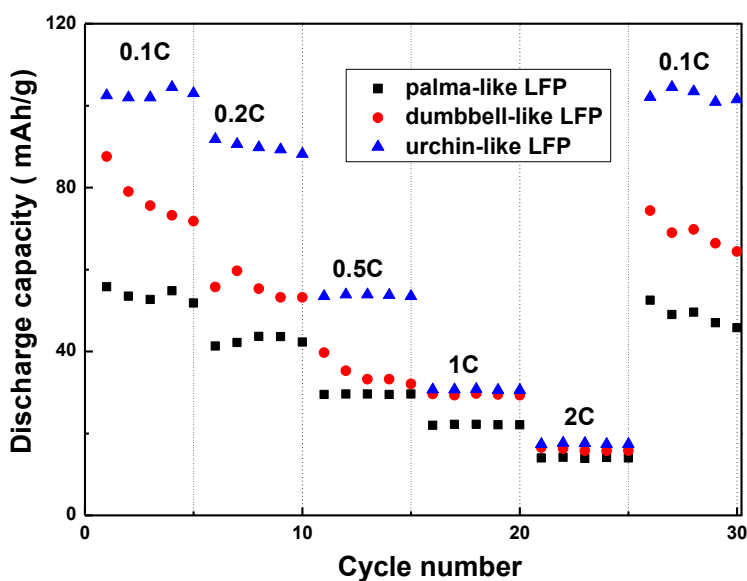


Figure 5. Lithium ion intercalation capacities of the three LiFePO_4 mesostructures at different discharge rates between 2.5 - 4.2V (vs. Li/Li^+)

Figure 5 shows the rate capability of all three hierarchical LFP mesostructures characterized under varied current densities for every 5 cycles. At lower current densities as 17 mA g^{-1} (0.1 C), 34 mA g^{-1} (0.1 C) and 85 mA g^{-1} (0.5 C), the three samples show great difference in discharge capacities. This situation should be attributed to the size difference of the structure and primary unit, which has obvious impact on the diffusion path of lithium ions and charge and mass transfer. The hierarchical urchin-like LFP mesostructures exhibited 101 mA h g^{-1} , 90 mA h g^{-1} and 54 mA h g^{-1} at different rate of 0.1 C, 0.2 C and 0.5 C, respectively. While lower capacity of 55 mA h g^{-1} , 41 mA h g^{-1} , 30 mA h g^{-1} and 80 mA h g^{-1} , 55 mA h g^{-1} , 35 mA h g^{-1} were obtained for palma-like and dumbbell-like LFP mesostructures with larger structure and building block sizes at the same rate of 0.1 C, 0.2 C and 0.5 C, respectively. However, when the current density increased to 170 mA g^{-1} (1 C) and 340 mA g^{-1} (2 C), the three hierarchical LFP mesostructures almost show the same lithium intercalation property. It is likely that the lithium ions do not have enough time to get into the interior crystals of LFP mesostructures and the size of the structures became dispensable when the current density increased higher than 170 mA g^{-1} . Thus, the effect from size of the whole structure and the prime units became insignificant under high rate condition. The rate performance of the urchin-like LFP mesostructures could not satisfy the practical application, even though this mesostructure has already occupied the prime position among those three samples. Since conductive coating is considered to be an effective way to improve the conductivity of the LFP materials, it is believed that the rate performance of these mesostructures could be enhanced after conductive coating. This is under investigation and will be reported later.

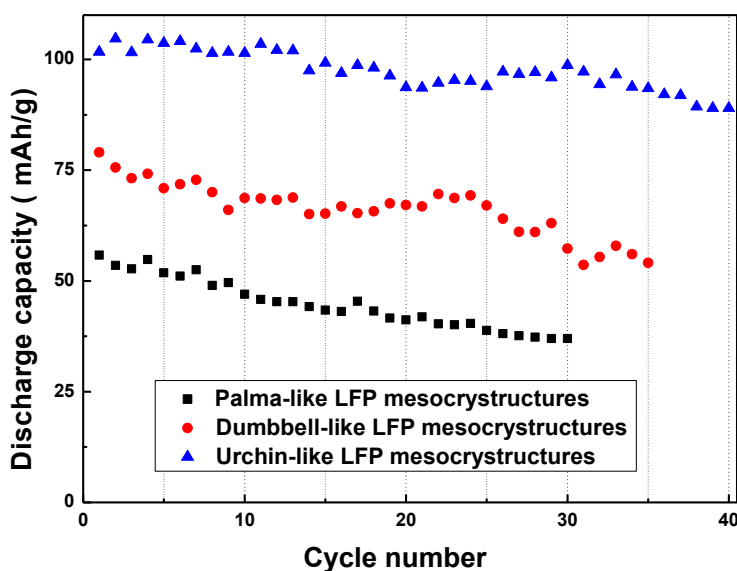


Figure 6. Cyclic performance of three LiFePO_4 mesostructures with various morphology at 0.1 C rate between 2.5 - 4.2V (vs. Li/Li^+)

Figure 6 shows the long-term cyclic performance of the three hierarchical LiFePO_4 mesostructures with different morphology at rate of 0.1 C. The discharge capacity of all three electrodes dropped fast. Only 66% capacity maintained after 30 cycles for the palma-like LFP

mesostructures and 68% capacity left after 35 cycles for the dumbbell-like LFP mesostructures. The urchin-like LFP mesostructures show the best cyclic stability among those three samples, the discharge capacity faded 12% after 40 cycles. Again, the cyclic performances of those three samples should be improved after conductive coating. The in situ carbon coating on these three hierarchical LFP mesostructures is under investigation and will be reported later.

4. CONCLUSIONS

Three dimensional hierarchical lithium iron phosphate mesostructures with different morphology were successfully synthesized via simple solvothermal route. EG/DMAC/H₂O mixture was utilized as co-solvent through the solvothermal process. No other surfactant or additive was applied during the synthesis. By varying the ratio of the EG/DMAC/H₂O co-solvent, hierarchical LiFePO₄ mesostructures with different morphology can be obtained. Palma-like, dumbbell-like and urchin-like hierarchical LiFePO₄ mesostructures with different small-sized composition units were successfully fabricated. The size of the whole mesostructure and the primary units has a great impact on the electrochemical performance of the products. Among the three LiFePO₄ mesostructures, the obtained urchin-like mesostructure with nano-sized LiFePO₄ plates composition units shows the best lithium intercalation and deintercalation properties without any conductive coating. The high specific surface area and high porosity brought by the special superstructure and well crystallized LiFePO₄ nano-plates composition units would facilitate to good lithium ion storage performance.

ACKNOWLEDGEMENT

NZ gratefully acknowledges fellowship from the China Scholarship Council. This research work has been financially supported in part by the National Science Foundation (NSF, CMMI-1030048) and the University of Washington TGIF grant.

Reference

1. A.S. Andersson, J.O. Thomas, B. Kalska, L. Haggstrom, *Electrochem. Solid-State Lett.*, 3 (2000) 66.
2. C. Wang, J. Hong, *Electrochem. Solid-State Lett.*, 10 (2007) A65.
3. M.S. Islam, D.J. Driscoll, C.A.J. Fisher, P.R. Slater, *Chem. Mater.*, 17 (2005) 5085.
4. C. Delacourt, L. Laffont, R. Bouchet, C. Wurm, J.B. Leriche, M. Morcrette, J.M. Tarascon, C. Masquelier, *J. Electrochem. Soc.*, 152 (2005) A913.
5. D. Morgan, A. Van der Ven, G. Ceder, *Electrochem. Solid-State Lett.*, 7 (2004) A30.
6. X. Zhi, G. Liang, L. Wang, X. Ou, L. Gao, X. Jie, *J. Alloy. Compd.*, 503 (2010) 370.
7. C.H. Mi, X.B. Zhao, G.S. Cao, J.P. Tu, *J. Electrochem. Soc.*, 152 (2005) A483.
8. Y.-S. Hu, Y.-G. Guo, R. Dominko, M. Gaberscek, J. Jamnik, J. Maier, *Adv. Mater.*, 19 (2007) 1963.
9. Z.-H. Wang, L.-X. Yuan, W.-X. Zhang, Y.-H. Huang, *J. Alloy. Compd.*, 532 (2012) 25.
10. D.Y. Wang, H. Li, S.Q. Shi, X.J. Huang, L.Q. Chen, *Electrochim. Acta*, 50 (2005) 2955.

11. X. Fang, J. Li, K. Huang, S. Liu, C. Huang, S. Zhuang, J. Zhang, *J. Solid State Electrochem.*, 16 (2012) 767.
12. P.P. Prosini, M. Carewska, S. Scaccia, P. Wisniewski, M. Pasquali, *Electrochim. Acta*, 48 (2003) 4205.
13. K.F. Hsu, S.Y. Tsay, B.J. Hwang, *J. Mater. Chem.*, 14 (2004) 2690.
14. L. Wang, Y. Huang, R. Jiang, D. Jia, *Electrochim. Acta*, 52 (2007) 6778.
15. V. Etacheri, R. Marom, R. Elazari, G. Salitra, D. Aurbach, *Energy Environ. Sci.*, 4 (2011) 3243.
16. J. Qian, M. Zhou, Y. Cao, X. Ai, H. Yang, *J. Phys. Chem. C*, 114 (2010) 3477.
17. H. Yang, X.L. Wu, M.H. Cao, Y.G. Guo, *J. Phys. Chem. C*, 113 (2009) 3345.
18. J. Popovic, R. Demir-Cakan, J. Tornow, M. Morcrette, D.S. Su, R. Schloegl, M. Antonietti, M.-M. Titirici, *Small*, 7 (2011) 1127.
19. D. Rangappa, K. Sone, T. Kudo, I. Honma, *J. Power Sources*, 195 (2010) 6167.
20. A.K. Padhi, K.S. Nanjundaswamy, J.B. Goodenough, *J. Electrochem. Soc.*, 144 (1997) 1188.
21. A.K. Padhi, K.S. Nanjundaswamy, C. Masquelier, S. Okada, J.B. Goodenough, *J. Electrochem. Soc.*, 144 (1997) 1609.
22. S.S. Zhang, J.L. Allen, K. Xu, T.R. Jow, *J. Power Sources*, 147 (2005) 234.
23. H. Liu, C. Li, H.P. Zhang, L.J. Fu, Y.P. Wu, H.Q. Wu, *J. Power Sources*, 159 (2006) 717.
24. X. Sun, J. Li, C. Shi, Z. Wang, E. Liu, C. He, X. Du, N. Zhao, *J. Power Sources*, 220 (2012) 264.
25. C.Y. Wu, G.S. Cao, H.M. Yu, J. Xie, X.B. Zhao, *J. Phys. Chem. C*, 115 (2011) 23090.
26. F. Deng, X.R. Zeng, J.Z. Zou, J.F. Huang, X.B. Xiong, X.H. Li, *J. Alloy. Compd*, 509 (2011) L324.
27. L. Wang, G.C. Liang, X.Q. Ou, X.K. Zhi, J.P. Zhang, J.Y. Cui, *J. Power Sources*, 189 (2009) 423.
28. H.-p. Liu, Z.-x. Wang, X.-h. Li, H.-j. Guo, W.-j. Peng, Y.-h. Zhang, Q.-y. Hu, *J. Power Sources*, 184 (2008) 469.
29. G. Arnold, J. Garche, R. Hemmer, S. Strobele, C. Vogler, A. Wohlfahrt-Mehrens, *J. Power Sources*, 119 (2003) 247.
30. K.S. Park, J.T. Son, H.T. Chung, S.J. Kim, C.H. Lee, H.G. Kim, *Electrochem. Commun.*, 5 (2003) 839.
31. M.R. Yang, W.H. Ke, S.H. Wu, *J. Power Sources*, 146 (2005) 539.
32. J.S. Yang, J.J. Xu, *Electrochem. Solid-State Lett.*, 7 (2004) A515.
33. Y.Q. Hu, M.M. Doeff, R. Kostecky, R. Finones, *J. Electrochem. Soc.*, 151 (2004) A1279.
34. S.F. Yang, P.Y. Zavalij, M.S. Whittingham, *Electrochem. Commun.*, 3 (2001) 505.
35. J. Chen, M.S. Whittingham, *Electrochem. Commun.*, 8 (2006) 855.
36. K. Saravanan, M.V. Reddy, P. Balaya, H. Gong, B.V.R. Chowdari, J.J. Vittal, *J. Mater. Chem.*, 19 (2009) 605.
37. M. Higuchi, K. Katayama, Y. Azuma, M. Yukawa, M. Suhara, *J. Power Sources*, 119 (2003) 258.
38. T. Muraliganth, A.V. Murugan, A. Manthiram, *J. Mater. Chem.*, 18 (2008) 5661.
39. A.V. Murugan, T. Muraliganth, A. Manthiram, *J. Phys. Chem. C*, 112 (2008) 14665.
40. N. Zhou, H.Y. Wang, E. Uchaker, M. Zhang, S.Q. Liu, Y.N. Liu, G. Cao, *J. Power Sources*, xxx (2013) xx-yy.
41. S.T. Myung, S. Komaba, N. Hirosaki, H. Yashiro, N. Kumagai, *Electrochim. Acta*, 49 (2004) 4213.
42. F. Teng, S. Santhanagopalan, A. Asthana, X. Geng, S.-i. Mho, R. Shahbazian-Yassar, D.D. Meng, *J. Cryst. Growth*, 312 (2010) 3493.
43. Y. Xia, W. Zhang, H. Huang, Y. Gan, J. Tian, X. Tao, *J. Power Sources*, 196 (2011) 5651.
44. J.-K. Kim, J.-W. Choi, G.S. Chauhan, J.-H. Ahn, G.-C. Hwang, J.-B. Choi, H.-J. Ahn, *Electrochim. Acta*, 53 (2008) 8258.
45. H. Zhang, G.R. Li, L.P. An, T.Y. Yan, X.P. Gao, H.Y. Zhu, *J. Phys. Chem. C*, 111 (2007) 6143.
46. J.Y. Luo, Y.G. Wang, H.M. Xiong, Y.Y. Xia, *Chem. Mater.*, 19 (2007) 4791.
47. H. Yang, X.L. Wu, M.H. Cao, Y.G. Guo, *J. Phys. Chem. C*, 113 (2009) 3345.
48. N. Meethong, H.Y.S. Huang, W.C. Carter, Y.M. Chiang, *Electrochem. Solid-State Lett.*, 10 (2007) A134.

49. P. Gibot, M. Casas-Cabanas, L. Laffont, S. Levasseur, P. Carlach, S. Hamelet, J.M. Tarascon, C. Masquelier, *Nat. Mater.*, 7 (2008) 741.
50. J. Wang, J. Polleux, J. Lim, B. Dunn, *J. Phys. Chem. C*, 111 (2007) 14925.
51. J. Maier, *Nat. Mater.*, 4 (2005) 805.
52. M. Winter, R.J. Brodd, *Chem. Rev.*, 105 (2005) 1021.

© 2013 by ESG (www.electrochemsci.org)